Adaptivity based on the constitutive error for the Maxwell's eigenvalue problem on polyhedral meshes

Matteo Cicuttin[1], Ruben Specogna[2], Francesco Trevisan[2]
[1]Université Paris-Est, Cermics (ENPC), F-77455 Marne-la-Vallée, France
[2]Polytechnic Department of Engineering and Architecture (DPIA), Università di Udine, 33100 Udine, Italy

This paper first introduces a simplified construction of the constitutive matrices for general polyhedral meshes. These constitutive matrices are geometrically defined by means of simple closed form expressions involving the geometric elements of the primal and dual meshes. Then, we solve for the first time the Maxwell's eigenvalue problem on general polyhedral meshes. In particular, we analyze the convergence of the eigenvalues when the mesh is adaptively refined by using the subgridding technique together with the constitutive inconsistency as error indicator.

Index Terms—**Maxwell eigenvalue problem, polyhedral meshes, adaptivity, Discrete Geometric Approach (DGA)**

I. Introduction

THE interest in discretization methods for electromagnetic problems on general polyhedral meshes has considerably grown recently. Polyhedral meshes, in fact, have the potential to allow faster and robust mesh generation and to enable novel techniques for adaptive mesh refinement and derefinement. In particular, the non-conforming-like refinement—as the subgridding proposed in [1]—and the adaptive coarsening strategy [2] are particularly appealing.

In this work we first introduce a set of simplified formulas to compute the Discrete Geometric Approach (DGA) constitutive matrices on arbitrary polyhedral meshes with planar faces. Then, we solve for the first time the Maxwell's eigenvalue problem on general polyhedral meshes and with two complementary formulations [3], [4], [5]. Finally, we investigate the effectiveness of using automatic mesh adaptivity in the modeling chain.

Given that the error estimation theory for full Maxwell problems is not yet as developed as the one for elliptic boundary value problems, we propose to use the constitutive inconsistency [3], [4] as error indicator. This does not provide guaranteed error bounds for any electromagnetic quantity, yet it has a clear physical ground. The idea is to refine the elements with the biggest difference in the electromagnetic solution provided by the two complementary formulations.

Another element of originality of this work is that for the first time we perform an automatic mesh refinement with subgridding. We remark that the subgridding we propose is not based on hanging nodes, like the ones already published in literature. In our case the subgridding without hanging nodes is enabled by using general polyhedral elements.

The paper is organized as follows. In Section II the complementary formulations of wave propagation problems are briefly reviewed and the technique we use for automatic mesh refinement based on the constitutive inconsistency is presented. Then, in Section III we introduce the novel geometrically defined constitutive matrices for polyhedral elements. Section IV shows the effectiveness of the proposed technique in the solution of a notoriously difficult problem.

Manuscript received Oct 12, 2016; accepted August 18, 2017. Date of current version April 22, 2017. Corresponding author: R. Specogna (e-mail: ruben.specogna@uniud.it).

Color versions of one or more of the figures in this paper are available online at http://ieeexplore.ieee.org.

Digital Object Identifier 10.1109/TMAG.2013.2281076

II. Complementary formulations

From time harmonic Maxwell's equations at angular frequency ω in a bounded domain Ω

$$\nabla \times \boldsymbol{e} = -i\omega \boldsymbol{b}, \qquad \nabla \times \boldsymbol{h} = i\omega \boldsymbol{d},$$

where $\boldsymbol{d}$, $\boldsymbol{e}$, $\boldsymbol{h}$, $\boldsymbol{b}$ are respectively electric displacement, electric, magnetic and magnetic induction fields together with the constitutive relations

$$\boldsymbol{d} = \boldsymbol{\epsilon} \boldsymbol{e}, \qquad \boldsymbol{h} = \boldsymbol{\nu} \boldsymbol{b},$$

where $\boldsymbol{\nu}$ and $\boldsymbol{\epsilon}$ are symmetric positive definite material tensors, the $\boldsymbol{e}$-formulation of electromagnetic wave propagation problem

$$\nabla \times (\boldsymbol{\nu} \nabla \times \boldsymbol{e}) - \omega^2 \boldsymbol{\epsilon} \boldsymbol{e} = \boldsymbol{0}, \tag{1}$$

can be derived. Similarly, the $\boldsymbol{h}$-formulation of the electromagnetic problem becomes

$$\nabla \times (\boldsymbol{\xi} \nabla \times \boldsymbol{h}) - \omega^2 \boldsymbol{\mu} \boldsymbol{h} = \boldsymbol{0}, \tag{2}$$

where $\boldsymbol{\xi} = \boldsymbol{\epsilon}^{-1}$ and $\boldsymbol{\mu} = \boldsymbol{\nu}^{-1}$. The corresponding eigenvalue problems [3], [4] are

$$\nabla \times (\boldsymbol{\nu} \nabla \times \boldsymbol{e}) = \omega^2 \boldsymbol{\epsilon} \boldsymbol{e}, \tag{3}$$

$$\nabla \times (\boldsymbol{\xi} \nabla \times \boldsymbol{h}) = \omega^2 \boldsymbol{\mu} \boldsymbol{h}. \tag{4}$$

A convenient technique to discretize these equations is the Discrete Geometric Approach (DGA), where (3) and (4) are written as

$$\mathbf{C}^T \mathbf{M}_\nu \mathbf{C} \mathbf{U} = \omega^2_{std} \mathbf{M}_\varepsilon \mathbf{U}, \tag{5}$$

$$\mathbf{C}^T \mathbf{M}_\xi \mathbf{C} \mathbf{F} = \omega^2_{compl} \mathbf{M}_\mu \mathbf{F}, \tag{6}$$

where $\mathbf{C}$ is the edge-face incidence matrix, $\mathbf{M}_\nu$, $\mathbf{M}_\varepsilon$, $\mathbf{M}_\xi$ and $\mathbf{M}_\mu$ are the constitutive matrices computed as described

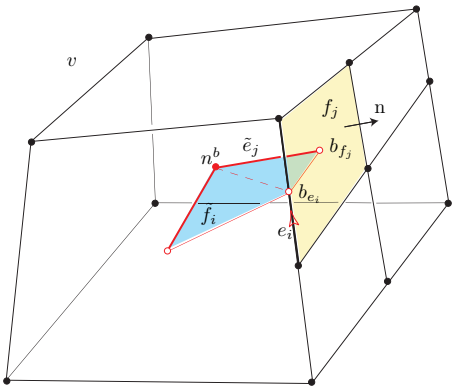

Fig. 1. Polyhedron v is shown together with the internal node n^b of the baricentric complex; n^b has an arbitrary location in v. An edge e_i, a face f_j and edge $\tilde{e}_j$, face $\tilde{f}_i$ of the barycentric complex are also shown. The barycenters b_{e_i} and b_{f_j} of edge e_i and of face f_j are drawn respectively.

in [1], ω is the angular frequency and $\mathbf{U}$ and $\mathbf{F}$ are the arrays of electromotive and magnetomotive forces on the mesh edges. The DGA is similar in spirit to the Finite Integration Technique (FIT) [6] but it is more general given that it allows to rigorously deal with arbitrary polyhedral elements.

Problems (3) and (4) are said to be the complementary formulations of the full Maxwell problem [3] and their solutions are obviously the same. In the discrete setting the two problems (5) (STD) and (6) (COMPL) give slightly different results due to the so-called *constitutive error* [3], [4], [5]. By exploiting this error, complementarity can be employed to perform adaptive mesh refinement, which results to be very effective in practice. That is, problems (5) and (6) are initially solved on a coarse mesh, which is then refined inside a standard adaptivity cycle according to the following error indicator for the generic element v

$$\Delta w_e = \int_v |\boldsymbol{e}_{std} - \boldsymbol{e}_{compl}|^2 dv, \tag{7}$$

where $\boldsymbol{e}_{std}$ and $\boldsymbol{e}_{compl}$ are the electric fields in the volume v computed by (5) and (6), respectively.

Since the automatic mesh refinement is performed with subgridding we need to construct constitutive matrices for arbitrary polyhedral elements. How to do that by means of a novel closed-form recipe is described in the following section.

III. Constitutive Matrices for General Polyhedra

A. Geometric elements of the polyhedral grid

We consider the geometric elements of a polyhedral grid restricted to a single polyhedron v shown in Fig. 1. We denote with e_i an oriented edge and with f_j an oriented face, where $i = 1, \ldots, N_e$, $j = 1, \ldots, N_f$ N_e, N_f being the number of edges and faces of v respectively. In Fig. 1 the oriented edge $\tilde{e}_j$ and oriented face $\tilde{f}_i$ of an interlocked grid are shown in addition; such a grid is denoted as *barycentric* grid since the barycenters b_{e_i} and b_{f_j} of e_i and of f_j are needed respectively for its construction. Finally, the internal node n^b has an arbitrary location in v. Vector e_i, denoted in roman type, is the edge vector[1] associated with e_i. Vector f_j is the face vector associated with the face f_j defined as $\mathrm{f}_j = \int_{f_j} \mathrm{n} ds$, where n is the unit vector normal to and oriented as f_j. Similarly vector $\tilde{\mathrm{f}}_i$ is the face vector associated with the face $\tilde{f}_i$ and $\tilde{\mathrm{e}}_j$ is the edge vector associated with the edge $\tilde{e}_j$. By construction, $\mathrm{e}_i \cdot \tilde{\mathrm{f}}_i > 0$ and $\mathrm{f}_j \cdot \tilde{\mathrm{e}}_j > 0$ hold. The only geometric hypothesis on v we assume, is that all edges and faces of the barycentric complex are contained in v. The volume V of v can be equivalently computed as $V = \frac{1}{3}\sum_{k=1}^{N_f} \mathrm{f}_k \cdot \tilde{e}_k = \frac{1}{3}\sum_{k=1}^{N_e} e_k \cdot \tilde{f}_k$.

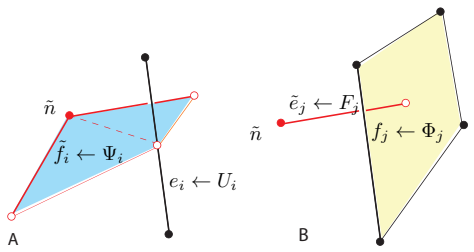

Fig. 2. Association between geometric elements and physical variables for the standard formulation.

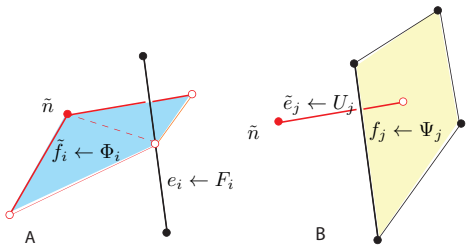

Fig. 3. Association between geometric elements and physical variables for the complementary formulation.

B. Association of physical variables to geometric elements

The physical variables, often referred to as degrees of freedom (dofs), involved in the standard (3) and in the complementary (4) formulations have a precise association to the geometric elements of the pair of interlocked grids. In Fig. 2 we summarize the association for the standard formulation, where the electro-motive force (e.m.f.) U_i is attached to e_i, the magnetic flux Φ_j to f_j, the magneto-motive force (m.m.f.) F_j to $\tilde{e}_j$ and the electric flux Ψ_i to $\tilde{f}_i$.

Similarly, in Fig. 3 we summarize the association for the complementary formulation obtained by simply swapping the role of the pair of grids. Therefore, the e.m.f. U_j is attached to $\tilde{e}_j$, the magnetic flux Φ_i to $\tilde{f}_i$, the m.m.f. F_i to e_i and the electric flux Ψ_j to f_j.

C. Constitutive matrices construction

In [1] we presented general expressions to compute symmetric positive definite and consistent local constitutive matrices for general polyhedra with planar faces, under the hypothesis of *piecewise uniform* fields. In this work we present an alternative and much simpler formulation of the expressions

[1]Its amplitude, direction and orientation coincide with the length, direction and orientation of e_i respectively.

presented in [1], based only on edge vectors, face vectors and inner products between them.

In the new formulas to compute the matrices $\underline{\mathbf{M}}_\nu$, $\underline{\mathbf{M}}_\varepsilon$, $\underline{\underline{\mathbf{M}}}_\nu$ and $\underline{\underline{\mathbf{M}}}_\varepsilon$, the material parameters reluctivity $\boldsymbol{\nu}$, permittivity $\boldsymbol{\varepsilon}$ and their inverses $\boldsymbol{\mu}$, $\boldsymbol{\xi}$ respectively are assumed uniform in the volume v.

These new formulas provide a new, straightforward recipe to build the constitutive matrices for DGA, both for the standard and for the complementary formulation.

1) Computation of $\underline{\mathbf{M}}_\nu$

Matrix $\underline{\mathbf{M}}_\nu$ maps the array $\mathbf{\Phi}$ of magnetic fluxes Φ_i attached to faces f_i onto the array $\mathbf{F}$ of m.m.f.s F_j attached to edges $\tilde{e}_j$ of the barycentric complex, with $i, j = 1, \ldots, N_f$. The entry $(\underline{\mathbf{M}}_\nu)_{ij}$ of $\underline{\mathbf{M}}_\nu$ can be written as

$$(\underline{\mathbf{M}}_\nu)_{ij} = \frac{1}{V}\,\tilde{\mathrm{e}}_i \cdot \boldsymbol{\nu}\tilde{\mathrm{e}}_j + \frac{1}{3}\sum_{k=1}^{N_f} \frac{\alpha_{ik}\,\alpha_{jk}}{\tilde{\mathrm{e}}_k \cdot \mathrm{f}_k}\,\tilde{\mathrm{e}}_k \cdot \nu\tilde{\mathrm{e}}_k, \tag{8}$$

where

$$\alpha_{ik} = \delta_{ik} - \frac{\tilde{\mathrm{e}}_i \cdot \mathrm{f}_k}{V} \tag{9}$$

holds, δ_{ik} being the Kronecker symbol.

2) Computation of $\underline{\mathbf{M}}_\varepsilon$

Matrix $\underline{\mathbf{M}}_\varepsilon$ maps the array $\boldsymbol{U}$ of voltages U_i attached to edges e_i onto the array $\mathbf{\Psi}$ of electric fluxes Ψ_j attached to faces $\tilde{f}_j$ of the barycentric complex, with $i, j = 1, \ldots, N_e$. The entry $(\underline{\mathbf{M}}_\varepsilon)_{ij}$ of $\underline{\mathbf{M}}_\varepsilon$ can be written as

$$(\underline{\mathbf{M}}_\varepsilon)_{ij} = \frac{1}{V}\,\tilde{\mathrm{f}}_i \cdot \boldsymbol{\varepsilon}\tilde{\mathrm{f}}_j + \frac{1}{3}\sum_{k=1}^{N_e} \frac{\beta_{ik}\,\beta_{jk}}{\tilde{\mathrm{f}}_k \cdot \mathrm{e}_k}\,\tilde{\mathrm{f}}_k \cdot \boldsymbol{\varepsilon}\tilde{\mathrm{f}}_k, \tag{10}$$

where

$$\beta_{ik} = \delta_{ik} - \frac{\tilde{\mathrm{f}}_i \cdot \mathrm{e}_k}{V} \tag{11}$$

holds, δ_{ik} being the Kronecker symbol.

3) Computation of $\underline{\underline{\mathbf{M}}}_\nu$

Matrix $\underline{\underline{\mathbf{M}}}'_\nu$ maps the array $\mathbf{F}$ of m.m.f.s F_j attached to edges $\tilde{e}_j$ of the barycentric complex onto the array $\mathbf{\Phi}$ of magnetic fluxes Φ_i attached to faces f_i, with $i, j = 1, \ldots, N_f$. The entry $(\underline{\underline{\mathbf{M}}}_\nu^{-1})_{ij}$ of $\underline{\underline{\mathbf{M}}}_\nu^{-1}$ can be written as

$$(\underline{\underline{\mathbf{M}}}_\nu^{-1})_{ij} = \frac{1}{V}\,\mathrm{f}_i \cdot \boldsymbol{\nu}^{-1}\mathrm{f}_j + \frac{1}{3}\sum_{k=1}^{N_f} \frac{\alpha_{ki}\,\alpha_{kj}}{\mathrm{f}_k \cdot \tilde{\mathrm{e}}e_k}\,\mathrm{f}_k \cdot \boldsymbol{\nu}^{-1}\mathrm{f}_k, \tag{12}$$

where for α_{ki} we use (9) swapping the indices. A second step, we invert $\underline{\underline{\mathbf{M}}}_\nu^{-1}$ obtaining a new local matrix $\underline{\underline{\mathbf{M}}}_\nu$ mapping the array $\mathbf{\Phi}$ onto the array $\mathbf{F}$.

4) Computation of $\underline{\underline{\mathbf{M}}}_\varepsilon$

Matrix $\underline{\underline{\mathbf{M}}}_\varepsilon^{-1}$ maps the array $\mathbf{\Psi}$ of electric fluxes Ψ_i attached to faces $\tilde{f}_i$ of the barycentric complex onto the array $\mathbf{U}$ of voltages U_j attached to edges e_j, with $i, j = 1, \ldots, N_f$. The entry $(\underline{\underline{\mathbf{M}}}_\varepsilon^{-1})_{ij}$ of $\underline{\underline{\mathbf{M}}}_\varepsilon^{-1}$ can be written as

$$(\underline{\underline{\mathbf{M}}}_\varepsilon^{-1})_{ij} = \frac{1}{V}\,\mathrm{e}_i \cdot \boldsymbol{\varepsilon}^{-1}\mathrm{e}_j + \frac{1}{3}\sum_{k=1}^{N_e} \frac{\beta_{ki}\,\beta_{kj}}{\mathrm{e}_k \cdot \tilde{\mathrm{f}}_k}\,\mathrm{e}_k \cdot \boldsymbol{\varepsilon}^{-1}\mathrm{e}_k, \tag{13}$$

where for β_{ki} we use (11) swapping the indices.

A second step, we invert $\underline{\underline{\mathbf{M}}}_\varepsilon^{-1}$ obtaining a new matrix $\underline{\underline{\mathbf{M}}}_\varepsilon$ mapping the array $\mathbf{U}$ onto the array $\mathbf{\Psi}$.

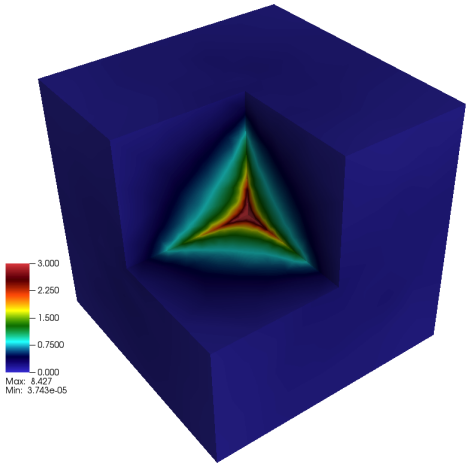

Fig. 4. The first eigenmode of the Fichera corner benchmark.

D. Geometric considerations on the matrices

Complementary formulations are obtained simply by swapping the association of the physical variables between the geometric elements of the two complexes. By looking at (5) and (6), it is possible to notice that the matrix $\mathbf{M}_\nu$ in the standard formulation plays the same role as $\mathbf{M}_\xi$ in the complementary formulation; the same goes for $\mathbf{M}_\varepsilon$ and $\mathbf{M}_\mu$. This happens because the pairs of matrices $\mathbf{M}_\nu$, $\mathbf{M}_\xi$ and $\mathbf{M}_\varepsilon$, $\mathbf{M}_\mu$ share the same geometric structure. In other words, $\mathbf{M}_\nu = \mathcal{M}_{\mathcal{S}\tilde{\mathcal{S}}}(\boldsymbol{\nu})$ and $\mathbf{M}_\xi = \mathcal{M}_{\mathcal{S}\tilde{\mathcal{S}}}(\boldsymbol{\xi})$ are two instances of the operator $\mathcal{M}_{\mathcal{S}\tilde{\mathcal{S}}}(\cdot)$ mapping from the primal surfaces to the dual edges, where only the material parameter changes. In the same way, $\mathbf{M}_\varepsilon = \mathcal{M}_{\mathcal{E}\tilde{\mathcal{S}}}(\boldsymbol{\varepsilon})$ and $\mathbf{M}_\mu = \mathcal{M}_{\mathcal{E}\tilde{\mathcal{S}}}(\boldsymbol{\mu})$ are two instances of the operator $\mathcal{M}_{\mathcal{E}\tilde{\mathcal{S}}}(\cdot)$ mapping from the primal edges to the dual surfaces, where only the material parameter changes.

Since these operators are not unique, different constructions are possible: using the argument just discussed, it is straightforward to compute the complementary matrices $\underline{\mathbf{M}}_\xi$, $\underline{\mathbf{M}}_\mu$, $\underline{\underline{\mathbf{M}}}_\xi$, $\underline{\underline{\mathbf{M}}}_\mu$ from (8), (10), (12) and (13) respectively.

IV. Numerical Results

To test the effectiveness of adaptivity we use the classical Fichera corner problem, which is notoriously difficult to solve [7], [8]. That is, the Maxwell's eigenvalue problem is solved in the domain $\Omega = (-1, 1)^3 \setminus [0, 1]^3$. The rapid field variation characterizing the solution of a problem of this kind makes it an excellent benchmark for adaptive refinement techniques, see Fig. 4. The reference solution 3.21988 for the first eigenvalue has been taken from [9], which considers a material with an electrical permittivity $\varepsilon_0\varepsilon_r = 1$, a magnetic permeability $\mu_0\mu_r = 1$ and perfect electric conductor boundary conditions.

The Intel MKL FEAST eigensolver was used to solve (5) and (6). We call as STD the solution of (5), whereas COMPL represents the solution of (6).

We first tested the proposed technique by using a tetrahedral mesh because tetrahedral mesh generators are nowadays well-integrated in the computer-assisted modeling chain. Here, the proposed technique shows comparable performances in terms of error vs number of DoFs with respect to a software

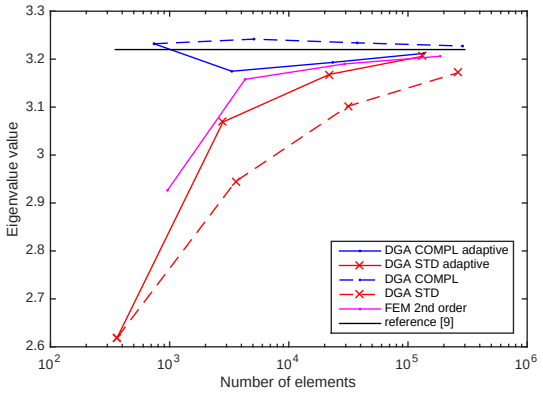

Fig. 5. Convergence of the first eigenvalue of the Fichera corner problem with tetrahedral meshes.

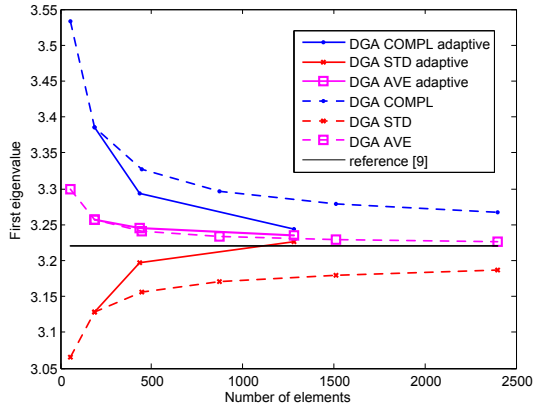

Fig. 6. Convergence of the first eigenvalue of the Fichera corner problem with polyhedral meshes.

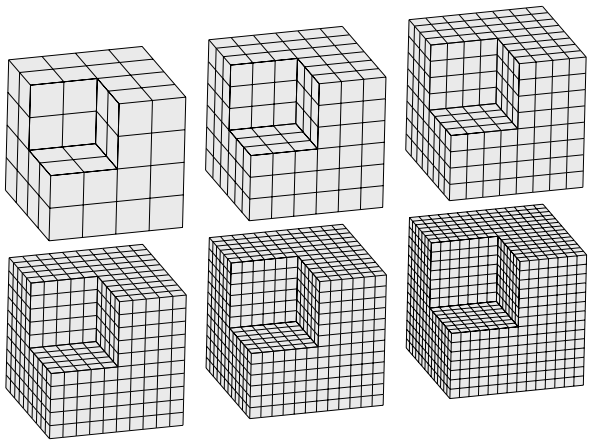

Fig. 7. Six hexahedral meshes uniformly refined.

implementing the second order Finite Element Method (FEM) that does not use mesh adaptivity, see Fig. 5. The same figure shows the improvement in the quality of the solution by using DGA with or without adaptivity. We remark that in this example the guaranteed bilateral energy bounds typical of complementarity applied to static electromagnetic problems [3] does not hold, showing once more as in [5] that bilateral bounds do not exist for full Maxwell problems.

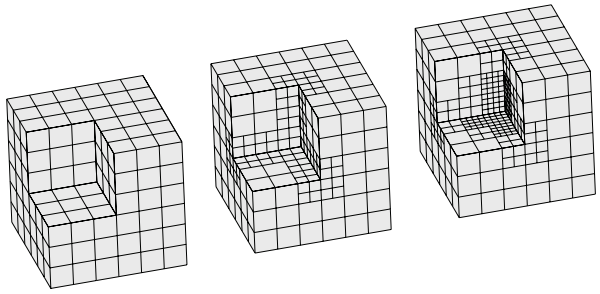

Fig. 8. Three meshes adaptively refined with subgridding.

In Fig. 6 we compare the convergence of the first eigenvalue obtained by considering six hexahedral meshes uniformly refined (Fig. 7) and by using three polyhedral meshes adaptively refined with subgridding (Fig. 8). Also in this case, adaptivity improves sensibly the quality of the solution. Here, AVG represents the average of the results of the STD and COMPL solutions.

Finally, we note that the solutions provided by using the constitutive matrices (8)-(10) or (12)-(13) provide roughly the same accuracy in the solution, therefore we used (8)-(10) since they do not require any element matrix inversion.

V. Conclusions

This paper introduced a new, simplified construction of the DGA constitutive matrices for general polyhedral meshes. This construction was used in the solution of the Maxwell's eigenvalue problem formulated as a pair of complementary formulations. The results on the Fichera corner problem show that the solution obtained by adaptively refining both tetrahedral and polyhedral meshes by using the constitutive error is improved with respect to the one obtained with a uniform refiniement of the mesh.

References

[1] L. Codecasa, R. Specogna, F. Trevisan, *A New Set of Basis Functions for the Discrete Geometric Approach*, J. Comput. Phys., Vol. 229, pp. 7401–7410, 2010.

[2] D.A. Di Pietro, R. Specogna, *An a posteriori-driven adaptive Mixed High-Order method with application to electrostatics*, J. Comput. Phys., Vol. 326, pp. 35-55, 2016.

[3] N.A. Golias, T.D. Tsiboukis, A. Bossavit, *Constitutive Inconsistency: Rigorous Solution of Maxwell Equations Based on a Dual Approach*, IEEE Trans. Magn., Vol. 30, No. 5, pp. 3586-3589, 1994.

[4] A. Bossavit, *Computational Electromagnetism: Variational Formulations, Complementarity, Edge Elements*, Academic Press, Boston, 1998.

[5] M. Cicuttin, L. Codecasa, R. Specogna, F. Trevisan, *Complementary discrete geometric h-field formulation for wave propagation problems*, IEEE Trans. Magn., Vol. 52, No. 3, 7202504, 2016.

[6] T. Weiland, *On the unique numerical solution of Maxwellian eigenvalue problems in three dimensions*, Particle Accelerators, Vol. 17, pp. 227-242, 1985.

[7] M. Costabel, M. Dauge, *Computation of resonance frequencies for Maxwell equations in non-smooth domains*, in Topics in Computational Wave Propagation: Direct and Inverse Problems, pp. 125-161, Springer Berlin Heidelberg, 2003.

[8] J. Bramble, T. Kolev, J. Pasciak, *The approximation of the Maxwell eigenvalue problem using a least-squares method*, Math. comp., Vol. 74, pp. 1575-1598, 2005.

[9] A. Buffa, G. Sangalli, *IsoGeometric Analysis: A New Paradigm in the Numerical Approximation of PDEs*, Springer Verlag, Berlin, 2012.